Optik - International Journal for Light and Electron Optics 174 (2018) 748–756

Contents lists available at ScienceDirect

Optik

journal homepage: www.elsevier.com/locate/ijleo

Original research article

Gradient sky scene based nonuniformity correction and local weighted filter based denoising

Rang Liu[a,b], Dejiang Wang[a,*], Ping Jia[a], Xin Che[a,b]

[a] *Key Laboratory of Airborne Optical Imaging and Measurement, Changchun Institute of Optics, Fine Mechanics and Physics, Chinese Academy of Sciences, Changchun, 130033, China*
[b] *University of Chinese Academy of Sciences, Beijing, 100049, China*

ARTICLE INFO

Keywords:
Nonuniformity correction
Gradient sky scene
Local weighted filter
Residual isolated noise

ABSTRACT

The nonuniformity of infrared focal plane array (IRFPA) seriously affects the image quality and the measurement accuracy of the infrared detector system. Long-wave infrared (LWIR) detector has highly sensitivity and image unstable factors, and the nonuniformity tends to drift slowly with the change of the environment. In this paper, we propose a new nonuniformity correction (NUC) algorithm based on gradient sky scene. Firstly, we obtain the two-point calibration images at two different pitch angles in the pure sky without any cloud. And then, the gain and offset coefficients are calculated from the standard two-point NUC. Finally, the local weighted filter based denoising algorithm is employed to eliminate a few residual isolated noise. Computational result shows that the SNR gain of the proposed method is increased 2.50 dB compared to the standard two-point method based on uniform blackbody. Results indicate that the proposed algorithm exhibits a superior correction effect and has the advantage of low complexity which meets the real-time requirements.

1. Introduction

Nowadays, the infrared focal plane array (IRFPA) technology has been widely applied to the thermal imaging system, infrared search and track (IRST) systems and external intrusion warning. IRFPA detector has the features of high sensitivity and high resolution compared with the scanning imaging system. However, the output response of all the detector arrays could not be exactly the same even for the uniform radiation, which is known as the response nonuniformity of IRFPA, due to the defective doping process, material mask, and optical system error [1–4]. There are also many defects on HgCdTe which could cause the nonuniformity, such as interstitial, Hg vacancy, etc. [5]. The nonuniformity of IRFPA can cause the fixed-pattern noise (FPN) and spatial noise which severely decrease the image quality and the accuracy of measurement system. Recent years, both domestic and foreign scholars launch much research on the nonuniformity correction (NUC) of IRFPA.

The commonly used NUC algorithms are mainly based on calibration and scene [6,7]. The correction factor of scene-based method is obtained by iterating the image sequence. At present, scene-based NUC methods mainly include temporal high-pass filtering, constant statistics, neural network method, and Kalman filtering [8–11]. However the algorithm complexity of the scene-based method is a little high, which making it difficult to perform real-time detection, and also this method may cause different degrees of ghosting. On the basis of principle of nonuniformity, the calibration-based method corrects each detector array to keep the output response be consistent at the same incident radiation. Generally, calibration-based method can obtain more accurate

* Corresponding author.
E-mail address: wangdj04@ciomp.ac.cn (D. Wang).

https://doi.org/10.1016/j.ijleo.2018.06.125
Received 8 October 2016; Received in revised form 16 April 2018; Accepted 27 June 2018

correction results. Since actual projects have higher requirements for real time and robustness, calibration method is widely used in particular the one-point and two-point NUC. But in the process of actual calibration we found that the blackbody calibration data on the ground is not very satisfactory to correct sky scene. As the different grayscale distribution between the blackbody and the sky scene, long-wave infrared detector (LWIR) is of poor stability and the nonuniformity tends to drift slowly. The nonuniformity noise appears again when the to-be-corrected point is out of the temperature range of blackbody calibration. And also, in-flight calibration usually requires additional devices (e.g., blackbody sources, electromechanical parts, etc.), which may increase the size and weight in aerial equipments [12].

In addition, the residual isolated noise affects the image quality and image interpretation seriously. So far, the most commonly image denoising methods include median filter, mean filter, wavelet denoising, and histogram based filters. Although these traditional filters can remove a portion of noise, they could also blur image details such as edge and texture information. Thus it is necessary to design an adaptive filter with by which the original signal information can be reserved well after denoising.

To solve these problems, we propose a novel NUC algorithm which integrating the gradient sky scene based NUC and the 4-direction weighted filter based denoising. The two-point calibration images are obtained by the infrared detector capturing at two different pitch angles in the pure sky scene instead of the blackbody data which obtained at two temperatures to perform two-point NUC. By employing the 4-direction weighted filter denoising algorithm, the residual noise will disappear further.

This paper is organized as follows. Section 2 describes the standard two-point NUC based on blackbody, and then a novel gradient sky scene based NUC is proposed. In Section 3, we present the local weighted filter algorithm to remove the residual nonuniformity noise. Section 4 shows the analysis and discussion about the proposed method. Finally, Section 5 offers the conclusion of the paper.

2. NUC based on gradient sky scene

2.1. Two-point NUC model

Two-point NUC is one of the basic correction methods of earlier research. Normally the response of IRFPA can be regarded as a linear model during a short period of time [13]. In the two-point NUC algorithm, the infrared detector's linear response model has the following expression [14]:

$$X_{ij}(\Phi) = \mu_{ij}\Phi + \nu_{ij}, \tag{1}$$

where μ_{ij} and ν_{ij} are respectively the gain and offset coefficients of pixel (i, j). Φ is the infrared radial flux, and $X_{ij}(\Phi)$ is the response value of (i, j).

Two-point NUC employs the blackbody at two different temperatures which are above and below the operation point so as to estimate the gain and offset coefficients of the linear model of response nonuniformity. The corrected response value by two-point NUC can be expressed through the following equation:

$$\begin{cases} Y(\Phi_L) = K_{ij}X_{ij}(\Phi_L) + B_{ij}, \\ Y(\Phi_H) = K_{ij}X_{ij}(\Phi_H) + B_{ij}, \end{cases} \tag{2}$$

where K_{ij} and B_{ij} are the calibration gain and offset coefficients of the detector. $X_{ij}(\Phi_L)$ is the output value of pixel (i, j) at a low temperature of the blackbody, and $X_{ij}(\Phi_H)$ is the output value of pixel (i, j) at a high temperature of the blackbody. $Y(\Phi_H)$ and $Y(\Phi_L)$ are average response values of $X(\Phi_H)$ and $X(\Phi_L)$ respectively. For each correction pixel (i, j), the values of K_{ij} and B_{ij} are fixed and will not vary with time within certain range, which are obtained from:

$$K_{ij} = \frac{Y(\Phi_H) - Y(\Phi_L)}{X_{ij}(\Phi_H) - X_{ij}(\Phi_L)}, \tag{3}$$

$$B_{ij} = \frac{Y(\Phi_H)X_{ij}(\Phi_L) - Y(\Phi_L)X_{ij}(\Phi_H)}{X_{ij}(\Phi_L) - X_{ij}(\Phi_H)}. \tag{4}$$

The two-point NUC algorithm has less computation and can achieve a real-time correction.

2.2. Two-point NUC based on blackbody

In the laboratory we use the focal length of 38 mm, Stirling refrigeration HgCdTe ST320 IRFPA detector whose response spectral band is 7.7–11.3 μm to obtain the blackbody calibration data, and the experimental equipment is shown in Fig. 1. The operating temperature of the detector is 77 K. The array format is 320 × 256 with the pixel size of 30 μm. The noise equivalent difference temperature (NEDT) of the FPA is 19 mK, and given for a 300 K scene temperature with the integration time of 250 μs. CI blackbody is employed to provide a stable radiant flux.

In order to obtain the reliable image resources, the IRFPA detector system to capture the scene images is also set up as presented in Fig. 2. The LWIR detector is mounted on the FLIR motion control systems, which is connected with the PC through a RJ45 Ethernet connector. The pan position and tilt position of the camera could be changed with E-series pan-tilt units.

By using the above equipment to capture the different sky scenes at different times, three original frames of image sequences are obtained as shown in Fig. 3(a)–(c), which present the serious FPN. Fig. 3(a) illustrates a single frame of the uncorrected sky scene

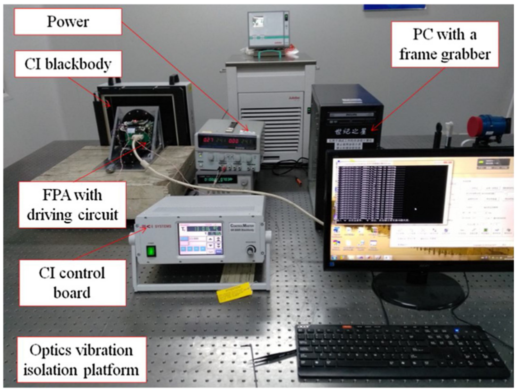

Fig. 1. Experimental equipment based on blackbody correction.

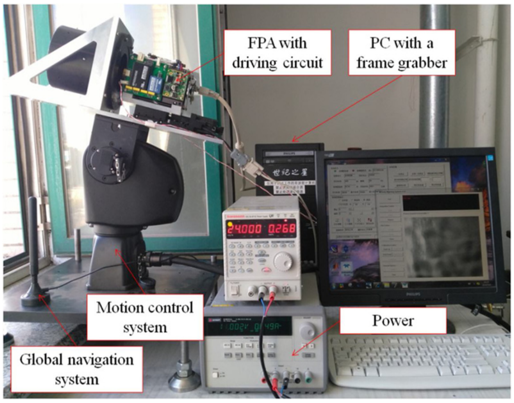

Fig. 2. Experimental equipment to capture scene images.

with a lot of cloud, and Fig. 3(b) shows a scene with sky and ground. Fig. 3(c) shows an uncorrected ground building scene. We employ the two-point NUC method based on blackbody calibration data which obtained in the laboratory before to correct the three original images. The NUC results are respectively shown in Fig. 3(d)–(f).

As can be seen from the above results, most fixed-pattern noise has disappeared. While the image quality is not very satisfactory, otherwise there is a lot of impulse noise appearing in Fig. 3(d). The two-point NUC based on blackbody is only accurate within narrow dynamic range. And the to-be-corrected point can easily reach out of the temperature scope of blackbody calibration if the correction coefficients are not updated in time, such as Fig. 3(e), which may produce the residual FPN.

2.3. The proposed NUC algorithm based on gradient sky scene

For the IRST system, the servo-control system adopts the working mode of sweep with a fixed pitch angle. The dynamic range of the captured images is relatively stable in a given area, and usually with the detector pitch angle growing big (the scene from the first row to the last row), the temperature gradually decreases and the gray value of the image shows a small gradient decline. So, the gray values of the first row and the last row may produce different values significantly. In the standard two-point NUC based on blackbody, an appropriate choice of the temperature of the blackbody may be the average temperature of the scene [15]. However, this may decrease the nonuniformity precision in the rows where the intensity values are far away from average value. A natural solution is employing a “gradient blackbody” by which the temperature matches the scene row by row.

Fortunately, the pure sky scene without cloud can be regarded as the “gradient blackbody”, whose grayscale distribution is consistent with the real to-be-corrected scene. On the basis of two-point NUC based on blackbody, we propose the gradient sky scene based NUC. The proposed method does not require cumbersome and expensive blackbody device, and only the two-point pure sky images below and above the to-be-corrected image are employed to obtain the gain and offset coefficients.

When capturing to-be-corrected image by the infrared detector shown in Fig. 2, the two-point T_1, T_2 images are obtained at the two different pitch angles below and above the to-be-corrected image in the pure and uniform sky scene without cloud. In order to suppress the temporal noise, 100 frames are captured and performed weighted average at each pitch angle. Let X_L and X_H be the T_1, T_2 images corresponding to the two-point below and above the to-be-corrected image, and Y_L, Y_H are their average response values respectively. From the above analysis, the response value of the two-point NUC based on gradient sky scene can be expressed as:

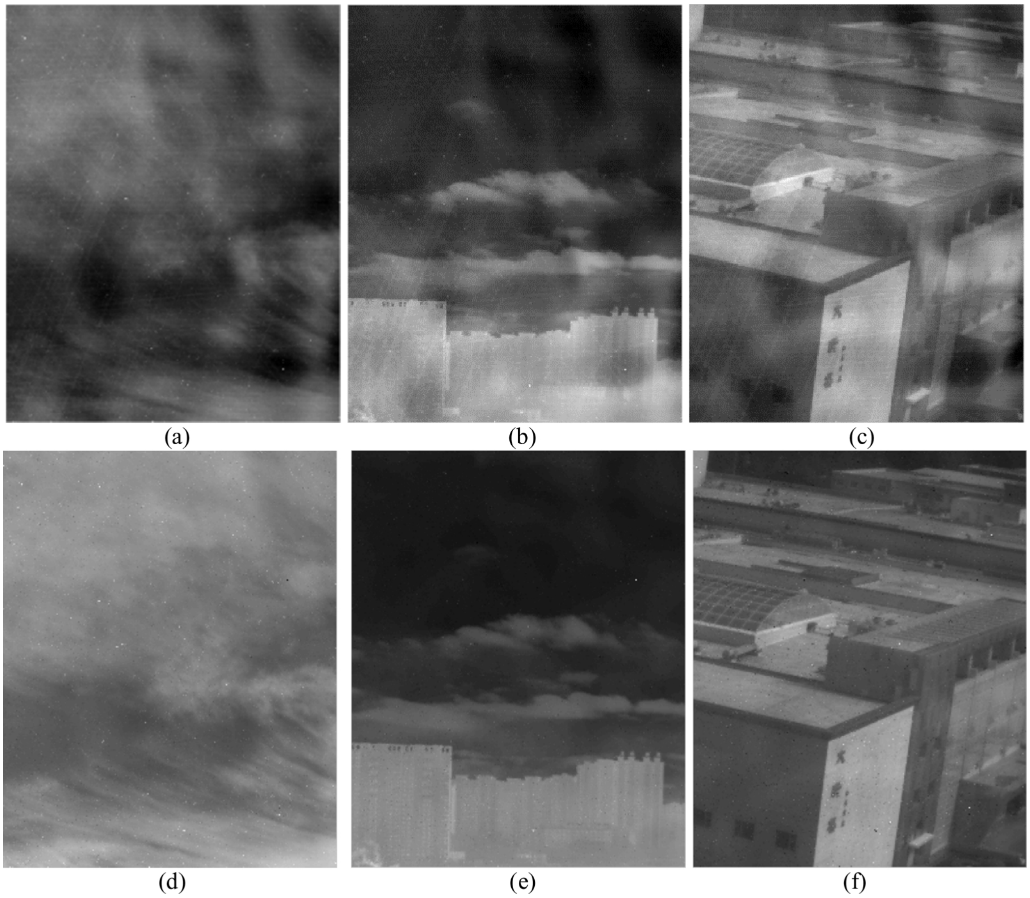

Fig. 3. Results of NUC based on blackbody. (a)–(c) Original image of only cloud, sky and building, and only building background respectively; (d)–(f) are results of (a)–(c) respectively after two-point NUC based on blackbody.

$$\begin{cases} Y_L = K'_{ij} \cdot X_{L,i,j} + B'_{ij}, \\ Y_H = K'_{ij} \cdot X_{H,i,j} + B'_{ij}. \end{cases} \tag{5}$$

Therefore, the calibration gain coefficient K' and offset coefficient B' can be obtained by putting T_1, T_2 images into the above expression, which are expressed as:

$$K'_{ij} = \frac{Y_H - Y_L}{X_{H,i,j} - X_{L,i,j}}, \tag{6}$$

$$B_{ij} = \frac{Y_H \cdot X_{L,i,j} - Y_L \cdot X_{H,i,j}}{X_{L,i,j} - X_{H,i,j}}. \tag{7}$$

Fig. 4 illustrates the correction results of three different sky scenes in Fig. 3, including T_1 images shown in Fig. 4(a)–(c), and T_2 images shown in Fig. 4(d)–(f), and finishing with the results of preliminary two-point correction present in Fig. 4(g)–(i). Obviously seen from the processing results of the two-point NUC based on gradient sky scene, the nonuniformity has been improved, and the FPN disappears completely. But there are still a few residual isolated noise which may be the residual nonuniformity according to three-dimensional image of Fig. 4(g) which is shown in Fig. 5.

In order to contrast the preliminary result of the gradient sky scene based NUC with the uniform blackbody based NUC, we calculate the global standard deviation (STD) of the NUC result of Fig. 3(a)–(c) by the two methods. The statistical results of three images are summarized in Table 1, and all the images are 14 bits.

3. Local weighted filter based denoising

Note that most of the nonuniformity noise in the image can be suppressed well by the above two-point NUC based on gradient sky scene with only a few isolated noise remained. According to the prior knowledge that the gray value of the isolated noise is always brighter than its 8-neighborhood pixels, thus we can detect out the points whose gray value are bright than their 8-neighborhood

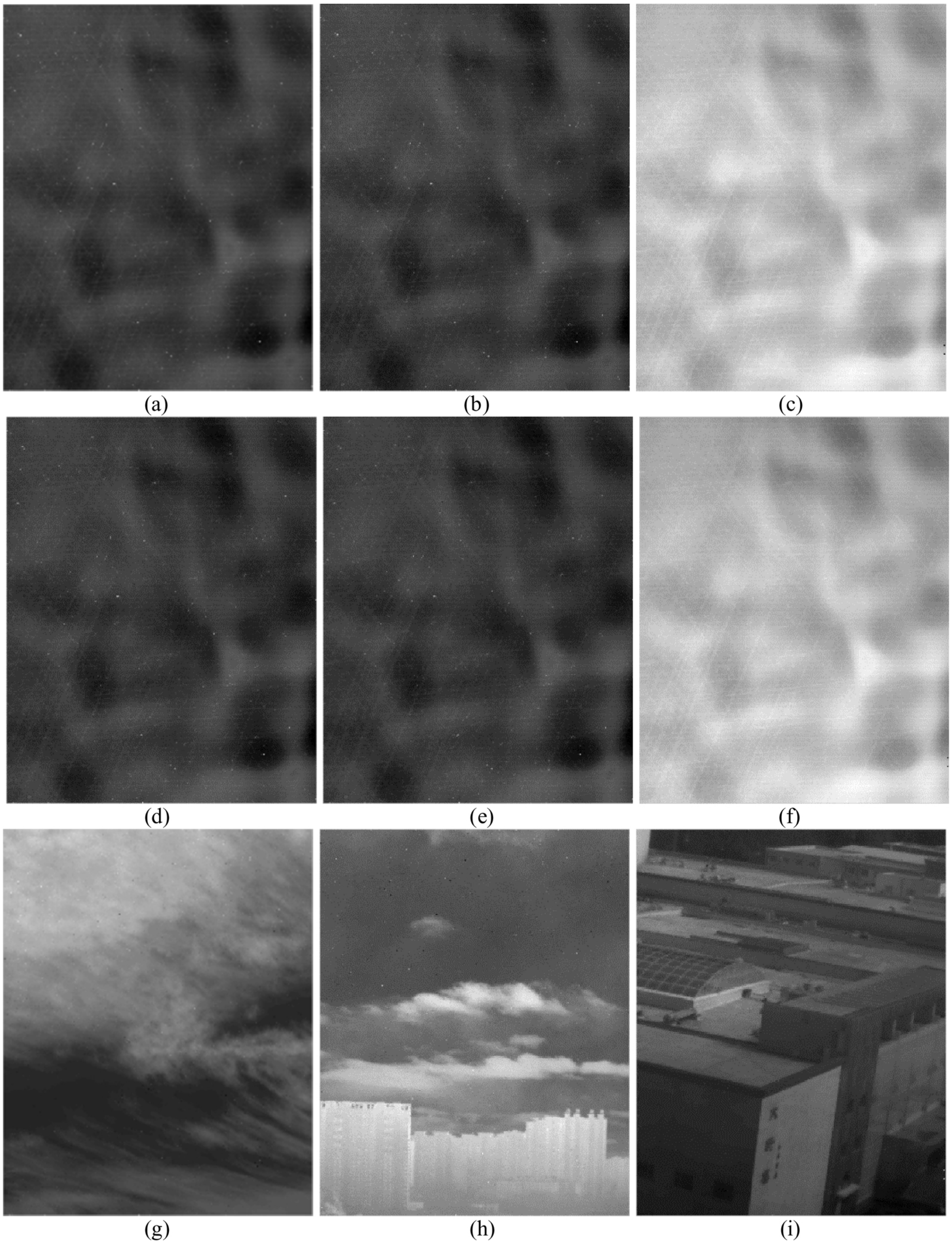

Fig. 4. Results of two-point NUC: (a)–(c) T1 temperature image; (d)–(f) T2 temperature image; and (g)–(i) results of preliminary correction.

pixels first. These detected points not only consist of the isolated noise, but some high-frequency edges of the cloud or building scene may also exist.

In order to distinguish the isolated noise from the high-frequency edges of the scene, the local 4-direction weighted filter algorithm is designed in the 5 × 5 window centered at $I(i, j)$ as shown in Fig. 6. We define L_m (m = 1–4) as the direction vector consisting of four coordinates around $I(i, j)$ in the mth direction, which is given in (8).

$$\begin{aligned} L_1 &= \{I(i-2, j-2), I(i-1, j-1), I(i+1, j+1), I(i+2, j+2)\} \\ L_2 &= \{I(i, j-2), I(i, j-1), I(i, j+1), I(i, j+2)\} \\ L_3 &= \{I(i+2, j-2), I(i+1, j-1), I(i-1, j+1), I(i-2, j+2)\}. \\ L_4 &= \{I(i-2, j), I(i-1, j), I(i+1, j), I(i+2, j)\} \end{aligned} \tag{8}$$

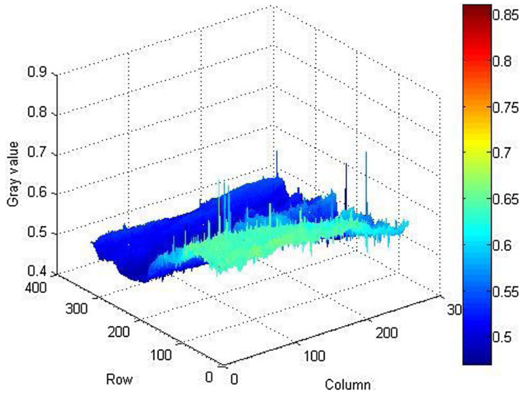

Fig. 5. Three-dimensional image of Fig. 4(g).

Table 1
Comparison of the global STD by two methods.

Method	Fig. 3(a)	Fig. 3(b)	Fig. 3(c)
Uniform blackbody	539	1884	731
Gradient sky scene	428	1672	615

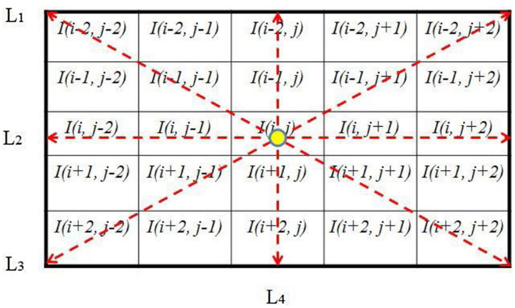

Fig. 6. 4-direction filter.

Then, the sum of the differences of gray values between $I(i+x, j+y)$ and $I(i, j)$ is calculated as follows:

$$d_{i,j}^{(m)} = \sum_{(x,y\in L_m)} w_{x,y} |I(i+x, j+y) - I(i, j)|, \tag{9}$$

where $w_{x,y}$ is the weighted kernel to describe the absolute difference between $I(i+x, j+y)$ and $I(i, j)$. We normally think that the closest 4-neighborhood pixels are more likely to the center pixel, so the larger weight 5/2 are assigned to them. We let $w_{x,y} = 2$ to the second closest pixels. And so on, we assign the small value 1 to the four far points whose coordinates x and y are both ± 2. L_1–L_4 are combined into a column vector L. The weighted kernel $w_{x,y}$ corresponding to elements of L are obtained as follows:

$$L = \begin{bmatrix} L_1 \\ L_2 \\ L_3 \\ L_4 \end{bmatrix}, \quad w_{x,y} = \frac{1}{28}\begin{bmatrix} 1 & 2 & 2 & 1 \\ \frac{3}{2} & \frac{5}{2} & \frac{5}{2} & \frac{3}{2} \\ 1 & 2 & 2 & 1 \\ \frac{3}{2} & \frac{5}{2} & \frac{5}{2} & \frac{3}{2} \end{bmatrix}, \tag{10}$$

A new variable named direction ratio (DR) is employed to distinguish the isolated noise from the high-frequency edges, which is calculated as the maximum of $d_{i,j}^{(m)}$ divided by the minimum of $d_{i,j}^{(m)}$ shown as follows:

$$\mathrm{DR} = \frac{\max(d_{i,j}^{(m)})}{\min(d_{i,j}^{(m)})}, (1 \le m \le 4) \tag{11}$$

When it comes to an edge pixel, there exist at least one very small $d_{i,j}^{(m)}$ and one very large $d_{i,j}^{(m)}$ because of the differences in four directions of th scene edge. Together, they give rise to a large DR. When it comes to an isolated noise, all the four direction differences of gray values are large and near-equal. Hence the DR of isolated noise is about 1.

Considering the different DR value, we can distinguish isolated noise from edges by setting a threshold of DR, and the choosing

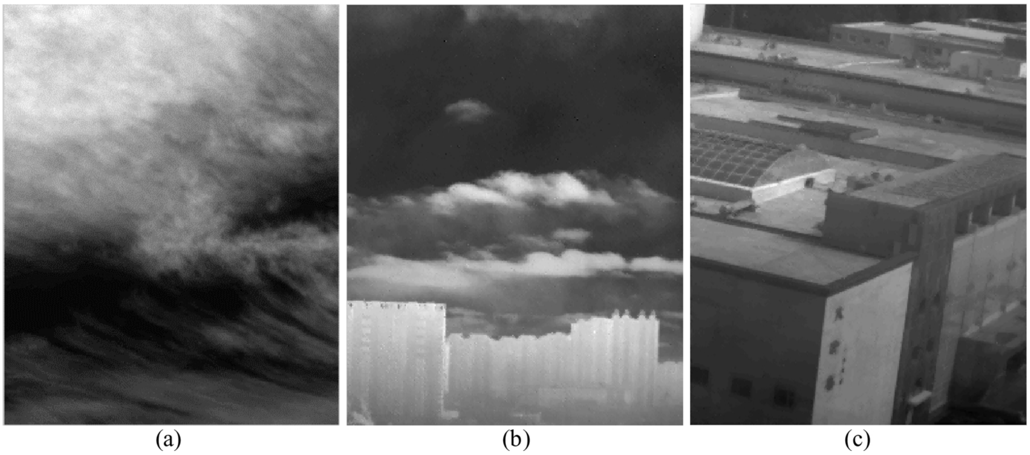

Fig. 7. Results of local weighted filter based denoising: (a) only cloud scene, (b) sky and building scene, and (c) only building scene.

threshold is slightly larger than 1. So we have the isolated noise detector as follows: if DR is less than the threshold, it is an isolated noise, otherwise it is an edge pixel. In order to visually display experimental results, the threshold is set to 1.5 in this paper.

After the above noise detection, most methods use median filtering in a small neighborhood to replace the noise. In this paper, we adopt the minimum variance method to perform the noise replacement. First, we calculate the standard deviation $\sigma_{i,j}^{(m)}$ (m = 1–4) of the isolated noise $I(i, j)$. Then find out the minimum standard deviation of the four $\sigma_{i,j}^{(m)}$ and gray values of the four coordinates corresponding to L_m, named I_1, I_2, I_3 and I_4. Their corresponding weighted kernels corresponding to $w_{x,y}$ are named w_1, w_2, w_3, and w_4, and the sum of the four weighted kernels are calculated as:

$$w = \sum_{i=1}^{4} w_i. \tag{12}$$

At last, we restore the noise pixel $I(i, j)$ as

$$I(i, j) = \frac{w_1}{w} I_1 + \frac{w_2}{w} I_2 + \frac{w_3}{w} I_3 + \frac{w_4}{w} I_4. \tag{13}$$

Through the above local weighted filter based denoising, we obtain the final denoising results shown in Fig. 7. The residual isolated noise has disappeared as can be seen from the following results. Through calculation, there are totally 37 residual non-uniformity noises be eliminated taking Fig. 7(b) as an example. In addition, the proposed algorithm could also enhance the image details and contrast.

4. Analysis and discussion

4.1. The gain K_{ij} and the offset B_{ij} compared by two methods

In order to further research the difference in gray distribution between the blackbody based NUC and the proposed gradient sky scene based NUC, we calculate the curves of gain K_{ij} (offset B_{ij}) via row (from low elevation to high elevation) in column 50 (j = 50) between the above two NUC methods, taking Fig. 3(a) the cloud scene as an example. Fig. 8(a) illustrates the curve of gain $K_{i,50}$ via the row. The gain $K_{i,50}$ fluctuates around 1 for the uniform blackbody based NUC, while for gradient sky scene based NUC, $K_{i,50}$ increases gradually from 0.6 to 1.6. Similarly, the offset $B_{i,50}$ fluctuates around 0 for uniform blackbody based NUC, while $B_{i,50}$ decreases gradually from 0.2 to -0.3 for gradient sky scene based NUC, which is shown in Fig. 8(b). Both of the gain $K_{i,50}$ and the gain $B_{i,50}$ for gradient sky scene based NUC present evident gradient variation from low elevation to high elevation, which is different from uniform blackbody based NUC.

4.2. Local standard deviation (STD) compared by two methods

The global STD can only be a rough evaluation index to describe the image quality when the image scene is very complex. Instead, we are more concerned about the local STD of each pixel in the whole image which calculated in its 5 × 5 pixels. The local STD can measure the roughness between the current pixel and its neighbors. If the local STD is relatively small, it can be determined as a better image quality, and also it demonstrates that the corresponding NUC method performs a better effect.

Also taking Fig. 3(a) as an example, the histograms of the local STD for the blackbody based and gradient sky scene based NUC are summarized in Fig. 9(a) and (b) separately, and the red curve in each figure is the fitting result of the histogram. For the blackbody based NUC, the histogram distributes range from 6 to 213, and the local STD corresponding to the peak of the histogram where distributes maximum number of pixels is about 31. For the gradient sky scene based NUC, the histogram distributes range from 0 to

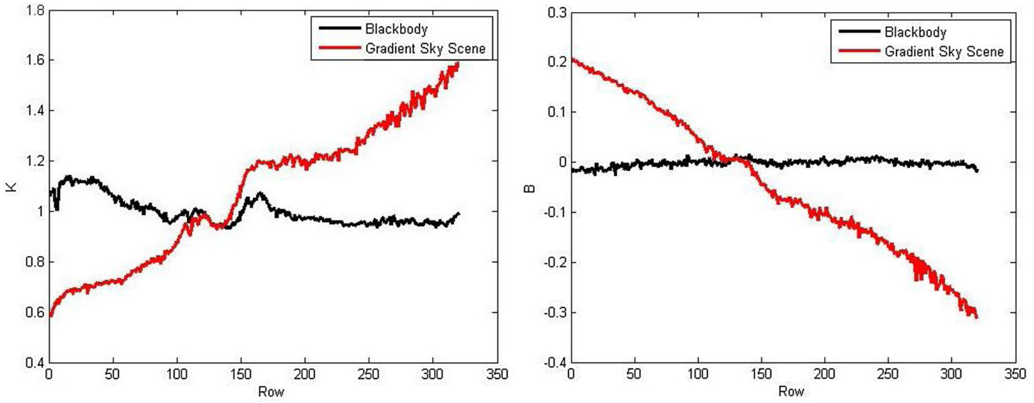

(a) (b)

Fig. 8. (a) the curve of gain K_{ij} via row, and (b) the curve of offset B_{ij} via row between the blackbody based NUC and the gradient sky scene based NUC.

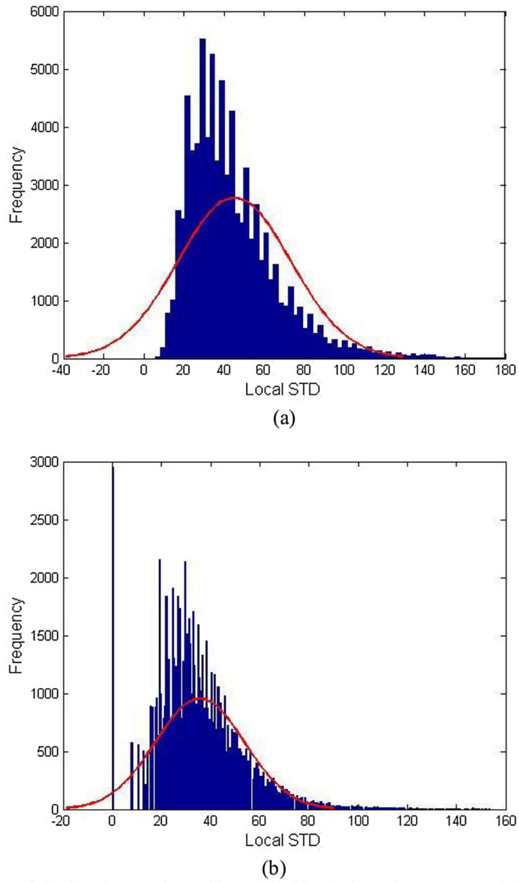

Fig. 9. The histogram of the local STD for uniform blackbody based NUC (a) and the proposed method (b). (For interpretation of the references to color in the text, the reader is referred to the web version of this article).

128, and the local STD corresponding to the peak of the histogram where distributes maximum number of pixels is near zero. If we just view from the histogram of the local STD, the proposed method consistently outperforms the standard two-point method. The following combination of the fitting curve, we make a concrete analysis between the proposed method and the standard two-point method. The local STD σ_1^2 corresponding to the peak of the fitting curve for the standard two-point method is 48. As for the proposed method, the local STD σ_2^2 corresponding to the peak of the fitting curve is 36, which is smaller than standard two-point method. The signal-to-noise ratio (SNR) gain is further obtained from the following definition formula (14). Computational result shows that the

SNR gain of the proposed method is increased 2.50 dB compared to standard two-point method based on blackbody. It can be evidently seen from the above analysis that the proposed algorithm has a better performance than the standard two-point NUC based on uniform blackbody.

$$G_{SNR} = 10\lg\frac{\sigma_1^2}{\sigma_2^2}. \tag{14}$$

4.3. Discussion

Inevitably, the algorithm has a limitation that it may be impossible to find a scene that is uniform in each row in the extreme weather such as the sky cover with a lot of cloud. If the nonuniform area is small, it may be most practical to replace the NUC coefficients of the polluted sections with the near uniform area at the same pitch angle. Worse yet, if the field of view is full of the nonuniform areas, the previous NUC coefficients may have similar performance for the infrared detector system. Maybe it is a better approach not to update the current NUC coefficients under such extreme weather [16].

5. Conclusions

The response nonuniformity of IRFPA seriously affects the measurement accuracy and imaging quality. Moreover, nonuniformity noise will shift with the change of working environment and time. Therefore the coefficients of NUC must be acquired in real time and real position. In this paper, we propose a new NUC algorithm based on gradient sky scene. We get two-point images at two different pitch angles in the pure sky. Then then gain and offset coefficients are obtained from two-point correction. The local 4-direction weighted filter algorithm is also employed to remove a few remaining isolated noise. Some experiments have been performed to test the proposed algorithm. Results verify the proposed method has a better performance than the two-point NUC based on blackbody.

Funding

This work was supported by the National Science Foundation (NSF) [grant numbers 61675202]; and the key Science-Technology Project of Jilin Province [grant numbers 11ZDGG001].

References

[1] Y. Yang, B.H. Shu, C.D. Zhang, et al., Application research in nonuniformity correction algorithm of IRFPA for infrared measuring system, Proc. SPIE vol. 9506, (2015) 950624.
[2] H. Yu, Z.J. Zhang, C.S. Wang, An improved retina-like nonuniformity correction for infrared focal-plane array, Infrared Phys. Technol. 73 (2015) 62–72.
[3] C. Zuo, Q. Chen, G.H. Gu, X.B. Sui, Scene based nonuniformity correction based on block ergodicity for infrared focal plane arrays, Optik – Int. J. Light Electron Opt. 123 (2012) 833–840.
[4] J. Ma, J. Zhao, Y. Ma, J. Tian, Non-rigid visible and infrared face registration via regularized Gaussian fields criterion, Pattern Recognit. 48 (2015) 772–784.
[5] J.W. Zhang, K.F. Mak, N. Nagl, et al., Multi-mW, few-cycle mid-infrared continuum spanning from 500 to 2250 cm^{-1}, Light: Sci. Appl. 7 (2018) 17180.
[6] J.G. Harris, Y.M. Chiang, Nonuniformity correction of infrared image sequences using the constant-statistics constraint, IEEE Trans. Image Process. 8 (1999) 1148–1151.
[7] S.N. Torres, J.E. Pezoa, M.M. Hayat, Scene-based nonuniformity correction for focal plane arrays by the method of the inverse covariance form, Appl. Opt. 42 (2003) 5872–5881.
[8] M.D. Nelson, J.F. Johnson, T.S. Lomheim, General noise processes in hybrid infrared focal plane arrays, Opt. Eng. 30 (1991) 1682–1700.
[9] D.A. Scribner, K.A. Sarkady, J.T. Caulfield, M.R. Kruer, G. Katz, C.J. Gridley, Nonuniformity correction for staring JR focal plane arrays using scene-based techniques, Proc. SPIE vol. 1308, (1990) 224–233.
[10] J. Zeng, X. Sui, H. Gao, Adaptive image-registration-based nonuniformity correction algorithm with ghost artifacts eliminating for infrared focal plane arrays, IEEE Photon. J. 7 (2015) 1–7.
[11] L. Geng, Q. Chen, W. Qian, An adjacent differential statistics method for IRFPA nonuniformity correction, IEEE Photon. J. 5 (2013) 6801615.
[12] Y.J. Liu, H. Zhu, Y.G. Zhao, Scene-based nonuniformity correction technique for infrared focal-plane arrays, Appl. Opt. 48 (2009) 2364–2372.
[13] D.L. Perry, E.L. Dereniak, Linear theory of nonuniformity correction in infrared staring sensors, Opt. Eng. 32 (1993) 1854–1859.
[14] A. Rossi, M. Diani, G. Corsini, A comparison of deghosting techniques in adaptive nonuniformity correction for IR focal-plane array systems, Proc. SPIE vol. 7834, (2010) 78340D.
[15] S. Kim, Two-point correction and minimum filter-based nonuniformity correction for scan-based aerial infrared cameras, Opt. Eng. 51 (2012) 106401.
[16] R.A. Leathers, T.V. Downes, R.G. Priest, Scene-based nonuniformity corrections for optical and SWIR pushbroom sensors, Opt. Express 13 (2005) 5136–5150.